PROTEINS
STRUCTURE ■ FUNCTION ■ BIOINFORMATICS

Global fold of human cannabinoid type 2 receptor probed by solid-state ^{13}C-, ^{15}N-MAS NMR and molecular dynamics simulations

Tomohiro Kimura,[1] Krishna Vukoti,[1] Diane L. Lynch,[2] Dow P. Hurst,[2] Alan Grossfield,[3] Michael C. Pitman,[4] Patricia H. Reggio,[2] Alexei A. Yeliseev,[1]* and Klaus Gawrisch[1]*

[1] Laboratory of Membrane Biochemistry and Biophysics, NIAAA, NIH, Bethesda Maryland 20892

[2] Department of Chemistry and Biochemistry, University of North Carolina, Greensboro, North Carolina 27402

[3] Department of Biochemistry and Biophysics, University of Rochester Medical Center, Rochester New York 14642

[4] Computational Biology Center, IBM Thomas J. Watson Research Center, Yorktown Heights, New York 10598

ABSTRACT

The global fold of human cannabinoid type 2 (CB_2) receptor in the agonist-bound active state in lipid bilayers was investigated by solid-state ^{13}C- and ^{15}N magic-angle spinning (MAS) NMR, in combination with chemical-shift prediction from a structural model of the receptor obtained by microsecond-long molecular dynamics (MD) simulations. Uniformly ^{13}C- and ^{15}N-labeled CB_2 receptor was expressed in milligram quantities by bacterial fermentation, purified, and functionally reconstituted into liposomes. ^{13}C MAS NMR spectra were recorded without sensitivity enhancement for direct comparison of C_α, C_β, and C=O bands of superimposed resonances with predictions from protein structures generated by MD. The experimental NMR spectra matched the calculated spectra reasonably well indicating agreement of the global fold of the protein between experiment and simulations. In particular, the ^{13}C chemical shift distribution of C_α resonances was shown to be very sensitive to both the primary amino acid sequence and the secondary structure of CB_2. Thus the shape of the C_α band can be used as an indicator of CB_2 global fold. The prediction from MD simulations indicated that upon receptor activation a rather limited number of amino acid residues, mainly located in the extracellular Loop 2 and the second half of intracellular Loop 3, change their chemical shifts significantly ($\geq$1.5 ppm for carbons and $\geq$5.0 ppm for nitrogens). Simulated two-dimensional $^{13}C_\alpha(i)$—$^{13}C{=}O(i)$ and $^{13}C{=}O(i)$—$^{15}NH(i+1)$ dipolar-interaction correlation spectra provide guidance for selective amino acid labeling and signal assignment schemes to study the molecular mechanism of activation of CB_2 by solid-state MAS NMR.

Proteins 2014; 82:452–465.

Key words: cannabinoid receptor; CB_2; GPCR; G protein-coupled receptor; solid-state NMR; molecular dynamics simulation.

INTRODUCTION

The cannabinoid CB_2 receptor is a member of the class A (rhodopsin family) of G protein-coupled receptors (GPCR). It is found primarily in tissues of immune and hematopoietic systems like spleen, tonsil, and thymus, where it controls function of immune cells.[1] Evidence has been presented that the CB_2 receptor is also present in brain, which makes the previous classification of CB_2 as peripheral cannabinoid receptor obsolete.[2] Experimental determination of the receptor structure is critical for elucidating molecular mechanisms of receptor function.

GPCR have a common structural motif of seven transmembrane α-helices which are alternately connected via intra- and extracellular loops. For several GPCR, the

Additional Supporting Information may be found in the online version of this article.

Grant sponsor: T.K, K.V., A.A.Y, and K.G. were supported by the Intramural Research Program of the National Institute on Alcohol Abuse and Alcoholism, National Institutes of Health. This work was supported in part by National Institutes of Health Grants RO1 DA003934 and KO5 DA021358 to P.H.R.

*Correspondence to: Alexei Yeliseev, Laboratory of Membrane Biochemistry and Biophysics, NIAAA, NIH, 5625 Fishers Lane, Room 3N-17, Bethesda, MD 20892-9410. E-mail: yeliseeva@mail.nih.gov (or) Klaus Gawrisch, Laboratory of Membrane Biochemistry and Biophysics, NIAAA, NIH, 5625 Fishers Lane, Room 3N-07, Bethesda, MD 20892-9410. E-mail: gawrisch@helix.nih.gov

Received 28 March 2013; Revised 12 August 2013; Accepted 21 August 2013
Published online 2 September 2013 in Wiley Online Library (wileyonlinelibrary.com).
DOI: 10.1002/prot.24411

structure at atomic resolution was recently unveiled by x-ray crystallography including bovine rhodopsin,[3–5] adenosine A_{2A} receptor,[6] β-adrenergic receptors,[7,8] CXCR4 chemokine receptor,[9] dopamine D3 receptor,[10] muscarinic acetylcholine receptors,[11,12] $S1P_1$ receptor,[13] histamine H_1 receptor,[14] nociceptin/orphanin FQ receptor,[15] opioid receptors,[16–18] protease activated receptor,[19] neurotensin receptor,[20] serotonin receptors,[21,22] smoothened receptor,[23] and glucagon receptor.[24]

Crystallographic results provided valuable information, such as the configuration of amino acid residues composing the ligand binding pocket, the arrangement of transmembrane helices, as well as the existence of amphipathic helix VIII near the intracellular end of helix VII. The recently published structure of a cocrystallized GPCR–G protein complex revealed the sites of interactions with G protein as well as the structural changes in GPCR upon activation.[25,26]

The availability of crystallographic data has stimulated interest and highlighted the necessity of studying structure and function of GPCR in their natural environment, the lipid bilayer, without conformational constraints from crystal packing.[27] Such experimental conditions are accessible by solid-state NMR spectroscopy. Recently, the chemokine receptor CXCR1 in DMPC bilayers was studied by solid-state NMR.[28] The secondary structure was obtained from measured and assigned chemical shifts of the backbone ^{13}C- and ^{15}N resonances of the protein. The global fold of the receptor was obtained by energy minimization using a homology model to rhodopsin with extensive experimental restraints from orientation-dependent ^{1}H-$^{13}C_\alpha$ and ^{1}H-^{15}N dipolar couplings.[28]

A prerequisite for structural studies by NMR is availability of purified, functional protein in the low milligram range. The expression levels of CB_2 receptor as well as of other GPCR in their natural host cells are quite low, except for visual rhodopsin that is highly concentrated in the disc membranes of retinal rod outer segment. Therefore, heterologous expression using mammalian-, insect-, yeast-, or bacterial cells as well as cell-free expression are used to produce the quantities of GPCR required for structural investigations.[29–31] Furthermore, for NMR studies the expression system must be adapted to efficiently incorporate stable ^{13}C, ^{15}N, isotopes into the target protein which requires modification of expression protocols. Isotope labeling of ligands, on the other hand, requires modified schemes of chemical synthesis.[27,32] Although a variety of expression hosts have been adapted to isotopic labeling, the use of a robust and efficient bacterial expression system is still the first choice for flexibility in planning of labeling schemes. *E. coli* cells grow well in minimal media of a defined composition which simplifies procedures for the incorporation of isotope-labeled precursors into the recombinant receptor.

Previously, we reported results on (i) *E. coli* expression of CB_2 receptor as a fusion with maltose binding protein (MBP) and removal of expression partners, (ii) chromatographic purification of the receptor at the level of milligrams,[33–35] (iii) stabilization of the receptor in micelles,[36] and (iv) detergent-free, homogeneous reconstitution into liposomes while maintaining function.[27] Large scale production of functional CB_2 receptor by fermentation of *E. coli* cells in a mineral salt medium (MSM) was also demonstrated.[37]

Here we report on expression, purification, and functional reconstitution of agonist CP-55,940-activated, uniformly ^{13}C-,^{15}N-labeled cannabinoid receptor CB_2 and first structural studies by solid-state NMR. We optimized expression conditions to produce uniformly ^{13}C-,^{15}N-labeled CB_2 receptor while minimizing the use of ^{13}C-labeled glucose. The latter is essential since yields of recombinant CB_2 per unit of biomass[37] are much lower than for soluble proteins or membrane proteins expressed as inclusion bodies. Typical expression protocols would have required quantities of ^{13}C-labeled glucose that are cost prohibitive. Uniform labeling of the receptor with ^{15}N is easily achieved by supplementation of the MSM with the relatively inexpensive ^{15}N-ammonium salts.

One-dimensional ^{13}C- and ^{15}N-MAS NMR spectra of the labeled CB_2 receptor were acquired for a quantitative comparison with simulated spectra derived from the atomic coordinates of MD simulations of the receptor.[38] The isotropic chemical shifts of proteins for the backbone $^{13}C_\alpha$-, $^{13}C{=}O$-, ^{15}NH-, and the side-chain $^{13}C_\alpha$-resonances reflect sensitively the amino acid sequence, secondary structure, side-chain conformations, and through-space interactions between amino acid residues.[39–45] Therefore, the chemical shift distribution of the recombinant CB_2 receptor measured by MAS NMR, containing contributions from resonances of all the 400 amino acid residues, is tightly linked to the global fold of the protein. Spin–spin (T_2) relaxation times were measured as well to calculate the relaxation linewidth of resonances. We also acquired two-dimensional $^{13}C{-}^{13}C$ and $^{13}C{-}^{15}N$ correlation spectra with the intention to resolve and assign resonances. However, for reasons discussed later, we did not achieve the required sensitivity and resolution that would have enabled assignment. Nevertheless, the measured distribution of chemical shifts, in particular the distribution of the C_α resonances reveals valuable information on the global fold of the recombinant CB_2.

The model of the CB_2 receptor employed here is based on the crystal structure of the Class A GPCR, rhodopsin in the dark-adapted state.[4] The rhodopsin structure was chosen as the template because no modifications were made to its structure in order to crystallize it. In addition, rhodopsin shares some unusual sequence motifs with the cannabinoid receptors, including the GWXC motif at the extracellular end of transmembrane helix IV that forms an aromatic stacking interaction with Y5.39.

This interaction affects the extracellular positions of transmembrane helices III–V and is therefore important for CB_2. We calculated low free energy conformations for any transmembrane helices with an important sequence divergence from rhodopsin. Specifically, in transmembrane helix II there is a pair of glycines that distort the helix while CB_2 has no equivalent distortion; similarly, residue 5.50 is a proline in rhodopsin but not in CB_2. The resultant model has been tested by substituted cysteine accessibility studies to identify residues that face into the CB_2 binding pocket,[46,47] by mutation to identify key ligand interactions sites,[46–49] and by covalent labeling of CB_2[50] to identify the method of ligand entry into the CB_2 binding pocket.

The CB_2 receptor model was then inserted into a lipid bilayer composed of 123 molecules of 1-palmitoyl-2-oleoyl-sn-glycero-3-phosphocholine (POPC) and 38 molecules of the endogenous ligand 2-arachidonyl-glycerol (2-AG).[38] A spontaneous binding of a 2-AG molecule from the lipid matrix to the ligand binding site observed in the simulations yielded the structure of agonist-activated CB_2 receptor that was compared with experimental results for agonist CP-55,940-bound receptor. The structure of CB_2 before 2-AG binding was defined as the inactive state of the receptor. Spectral prediction was performed using the programs SHIFTX[51] and SPARTA,[52] which calculate the chemical shift values semiempirically based on databases of previously reported protein structures with resonance assignments. The sensitivity of spectra to changes in the primary amino acid sequence and to secondary structure is demonstrated.

The experiments and spectral predictions are useful for developing strategies for specific labeling of amino acids that are likely to yield well resolved and assigned resonances in multidimensional NMR experiments. The CB_2 model was also used to show that selective amino acid labeling schemes can be used for elucidation of mechanisms of receptor activation.

MATERIALS AND METHODS

Information on chemicals, the protein expression protocol including composition of media, protein purification and reconstitution, and molecular dynamics calculations are provided in the Supporting Information.

^{13}C MAS NMR

The proteoliposomes containing uniformly ^{13}C-, ^{15}N-labeled CB_2 receptor were pelleted by ultracentrifugation at 417,200*g* for 12 h at 4° C. The pellet was transferred to a 4-mm MAS rotor with a 50-μL sample volume sealed by a Kel-F insert (Bruker BioSpin, Billerica, MA). The ^{13}C MAS NMR spectra of proteoliposomes were recorded at a ^{13}C resonance frequency of 201.21 MHz on an AV800 spectrometer equipped with a 4-mm ^{1}H/^{13}C/^{15}N MAS variable-temperature probehead (Bruker BioSpin). Measurements were carried out at MAS frequencies of 10 and 15 kHz. The sample temperature was varied from 9 to 26° C. Spectra were acquired without sensitivity enhancement by crosspolarization or the nuclear Overhauser effect using a 5.0-μs 90° pulse on ^{13}C and a ^{1}H decoupling power of $(\gamma/2\ \pi)B_1 = 56.7$ kHz in a spinal-64 sequence applied during ^{13}C detection. Typically 24,000 scans with 1024 data points were acquired at a dwell time of 8.3 μs and a 2-s delay time between scans. The free-induction decay signals were processed with an exponential window function corresponding to a line broadening of 50 Hz upon Fourier transformation. For subtraction of the natural abundance ^{13}C resonances of lipids, spectra with a transverse-relaxation (T_2) filter (Hahn echo) were acquired. The echo delay time was varied from 0.5 to 5.0 ms. A delay time of 3.0 ms resulted in an almost complete decay of protein resonances with only modest attenuation of lipid resonances that decay much slower. After intensity adjustment to account for the relaxation decay, this lipid spectrum was subtracted from the spectrum recorded without the relaxation filter and yielded a ^{13}C spectrum of CB_2 receptor almost free from contributions of lipid resonances. The ^{13}C-chemical shift scale was calibrated in reference to DSS (sodium 2,2-dimethyl-2-silapentane-5-sulfonate) by setting the choline γ signal of PC to 57.6 ppm.[53,54]

^{15}N MAS NMR

A ^{1}H-^{15}N crosspolarization (CP) MAS NMR spectrum of the CB_2 proteoliposomes was recorded on an AV800 spectrometer at a ^{15}N resonance frequency of 81.08 MHz, 10 kHz MAS, 18° C, 3.7-μs ^{1}H 90° pulse, 1-ms ^{1}H-^{15}N crosspolarization at $(\gamma/2\pi)B_1 = 50$ kHz with a 100–80% linear ramp on the ^{1}H channel, $(\gamma/2\pi)B_1 = 60$ kHz ^{1}H decoupling during ^{15}N detection using a spinal-64 sequence, 30,000 scans, 1024 data points at a dwell time of 5 μs, and 2-s delay time between scans. The ^{15}N-chemical shift scale was calibrated by setting the midpoint of the ^{15}N-amide resonance to 120 ppm.

^{13}C- and ^{15}N chemical-shift prediction

The atomic coordinates of the CB_2 receptor were obtained from microsecond-long molecular dynamics simulations of CB_2 receptor in a lipid matrix as explained in the Introduction section.[38] An abbreviated description of simulation procedures is provided in Supporting Information. The ^{13}C-, and ^{15}N-chemical shifts of C_α-, C_β-, C═O-, and NH-resonances of the CB_2 receptor were predicted based on the atomic coordinates of the receptor obtained in MD simulations using the shift-prediction programs SHIFTX[51] and SPARTA.[52] The programs yield the shift values referenced to 4,4-

dimethyl-4-silapentane-1-sulfonic acid (DSS). The prediction was performed on the ligand-free inactive and agonist-bound activated states of CB_2 receptor from the simulations.[38] The chemical-shift value at each atomic site was calculated as the average from five or six time points taken at intervals of 0.9 or 1 ns of the simulations. The predicted chemical shift values are expected to be accurate within standard deviations of 1.4 ppm for ^{13}C- and 3 ppm for ^{15}N-resonances when applied to membrane proteins.[55] The ^{13}C spectra were simulated using the predicted C_α, C_β, and C═O chemical shifts and assuming a linewidth of resonances of 100 Hz. In the chemical-shift prediction, the eleven histidines in wild-type CB_2 receptor were treated as deprotonated as required by programs for chemical shift prediction. For recombinant CB_2 receptor[35] (see Supporting Information Fig. S4 for amino acid sequence), the 12 histidines in the N- and C termini were also treated as deprotonated, and all amino acids in the termini were assumed to be in random coil conformation. The number of histidines is modest compared to the total number of residues (11 of 360 total in the wild type sequence, and 23 of 400 in recombinant CB_2-130). A comparison of simulated spectra for wild-type CB_2 and recombinant CB_2-130 suggested that the influence of histidines and their state of protonation on the shape of ^{13}C resonance bands is insignificant (see Supporting Information Fig. S3).

RESULTS AND DISCUSSION

Expression, purification, and reconstitution of ^{13}C-, ^{15}N-CB_2 receptor

Fermentation of *E. coli* BL21-21(DE3) harboring plasmid pAY130 for expression of ^{13}C- and ^{15}N-labeled recombinant CB_2 receptor[35] was performed in MSM containing ^{13}C-labeled glucose as the sole carbon source and $^{15}NH_4Cl$ as the sole nitrogen source, and produced high density biomass that yielded ~6 mg of uniformly ^{13}C-,^{15}N-labeled, MBP-CB_2 fusion protein in the functional state. The fusion protein was solubilized from bacterial plasma membranes in a mixture of detergents CHAPS, *n*-dodecyl-β-D-maltopyranoside (DDM), and cholesteryl hemisuccinate (CHS) with addition of cannabinoid agonist CP-55,940.[36] Upon purification of the fusion protein on a Ni-NTA column, the MBP expression partner was removed by treatment with TEV protease. CB_2 was further purified by affinity chromatography on a StrepTactin resin as described previously.[35]

Reconstitution of the purified, uniformly ^{13}C-,^{15}N-labeled CB_2 receptor (2.8 mg) with phospholipids (28 mg; POPC/POPS = 4/1, mol/mol) by the rapid-dilution method yields detergent free, homogeneous proteoliposomes.[27] The recovery of protein and lipids in the proteoliposome preparation was high: 2.6 mg (92% yield) of the ^{13}C-, ^{15}N-labeled CB_2 and 33.3 mg of lipids (nearly 100% yield). In addition to the POPC and POPS, the lipid matrix also contained the CHS that was added to micellar solutions of CB_2 to prevent denaturation of the receptor and was almost quantitatively incorporated into proteoliposomes upon detergent removal. The molar ratio of protein and lipids in proteoliposomes was CB_2/POPC/POPS/CHS, 1/505/120/150.[27] Ligand-binding experiments by solid-state ^{2}H MAS NMR using selectively ^{2}H-labeled CP-55,940-d_6[32] revealed that >90% of reconstituted CB_2 receptor is ligand-binding competent.[27] The agonist-bound ^{13}C-, ^{15}N-CB_2 receptor activated G proteins accordingly in an *in vitro* coupled assay.[27,33,35]

^{13}C MAS NMR

The NMR experiments were conducted on proteoliposomes in PBS buffer containing 2.6 mg of uniformly ^{13}C-, ^{15}N-labeled CB_2 receptor as described above, activated with agonist CP-55,940. Detection of ^{13}C-resonances was performed without sensitivity enhancement such as cross-polarization, INEPT, or the nuclear Overhauser effect to ensure that intensities of all ^{13}C-resonances of the protein are identical to enable a quantitative comparison of predicted spectra from molecular simulations and experimental results. The relaxation delay between acquisitions was sufficiently long to avoid intensity losses due to saturation.

The measured ^{13}C-spectrum is presented in Figure 1(a). The spectrum shows bands of superimposed resonances; each band represents different carbon sites[39,42,43,54,56] of the CB_2 receptor: side-chain aliphatic, 10–45 ppm; C_α, 45–70 ppm; side-chain aromatic, 110–140 ppm; Arg C_ζ, Tyr C_4 160 ppm; C═O, 175–180 ppm. The bands are accompanied by MAS side bands of much lower intensity located at multiples (n = 1,2,...) of the MAS frequency from the center bands. In Supporting Information Figure S1, the locations of the side bands recorded at MAS frequencies of 10 and 15 kHz are shown. At 15 kHz, the C_α and C═O resonances which are highly sensitive to the global fold of the backbone, can be analyzed without interference from side bands of other carbon sites. The well-resolved signals on top of the resonance bands of CB_2 in Figure 1(a) are natural-abundance ^{13}C resonances of lipids in the fluid phase. The lipid resonances have much longer transverse (T_2) relaxation times than the protein resonances. Therefore, a spectrum showing only lipid resonances can be obtained by application of a T_2-filter that effectively suppresses protein resonances [Fig. 1(b)]. The experiments also yielded the T_2 relaxation times of lipids which permitted correction of their intensities for relaxation decay. The corrected lipid spectrum was then subtracted from the combined spectrum of protein and lipids [Fig. 1(a)] to yield the ^{13}C spectrum of pure CB_2 receptor [Fig. 1(c)]. Experiments were conducted in the temperature range of 9–26° C, above the gel-fluid phase transition of the lipid matrix. No changes in spectral appearance as a

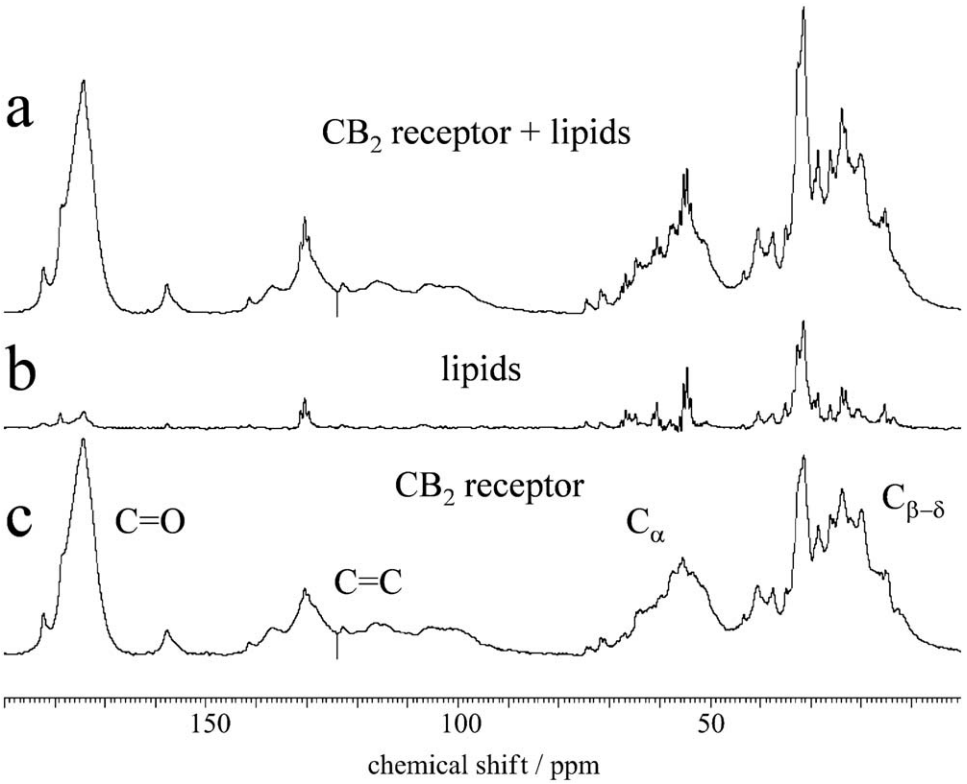

Figure 1

(**a**) ^{13}C MAS NMR spectrum of the agonist-bound active state of the ^{13}C-,^{15}N-CB$_2$ receptor in liposomes. (**b**) The lipid spectrum observed by application of a T_2 filter, to remove the protein signals, was subtracted from the total spectrum (CB$_2$ receptor + lipids) to yield (**c**) the spectrum of CB$_2$ receptor. The measurements were conducted at 9° C and a MAS frequency of 15 kHz. The delay time in the Hahn echo sequence was set to 3.0 ms. The molar ratios of the protein and lipids in the proteoliposomes are CB2/POPC/POPS/CHS, 1/505/120/150.

function of temperature were observed (Supporting Information Fig. S2).

The T_2 relaxation experiments indicated that the C_α and C═O bands have relaxation times of 2.8 and 4.2 ms, respectively (Fig. 2), equivalent to a resonance linewidth at half height of 0.55 and 0.40 ppm. The actual linewidth could be somewhat larger due to inhomogeneous line broadening. The intrinsic resolution on the order of 0.5 ppm is encouraging for designing schemes of selective-isotope labeling of CB$_2$ receptor that may yield resolved resonances with their assignments; see discussion below. The large number of resonances of the 44-kDa recombinant, uniformly ^{13}C-, ^{15}N-labeled protein in combination with the limited resolution resulted in heavy signal superposition. Nevertheless, the shape of the band of superimposed resonances reports important information on receptor fold as will be presented below. This applies in particular to the band of C_α resonances which has a rather wide distribution of chemical shifts.

^{15}N MAS NMR

The ^{15}N MAS NMR spectrum of ^{13}C-, ^{15}N-CB$_2$ receptor recorded with sensitivity enhancement by ^{1}H-^{15}N crosspolarization is shown in Figure 3 with signal assignments. Note that detection of the ^{15}N resonances (sensitivity $\propto \gamma^3$, where γ is the gyromagnetic ratio) at the protein concentration of our experiments requires sensitivity enhancement by ^{1}H-^{15}N crosspolarization. The spectrum is largely dominated by the band of backbone amide resonances centered at 120 ppm. Superimposed on the backbone amide resonances are side-chain ^{15}N resonances of tryptophan indole, asparagine and glutamine amides, as well as backbone ^{15}N resonances of the proline ring. The side-chain resonances of arginines and lysines upfield from the amide band were well resolved, and the side-chain resonances of histidines appear downfield. The backbone amide band plays a key role for ^{13}C resonance assignments when site-selectively isotope-labeled CB$_2$ receptor is investigated.

Multidimensional NMR experiments

2D CP-DARR ^{13}C-^{13}C correlation experiments[57] were acquired with mixing times from 50 to 300 ms. Furthermore, we conducted 2D ^{15}N-^{13}C correlation experiments[58] yielding a selective transfer of the ^{15}N magnetization to directly bonded ^{13}C nuclei (results not

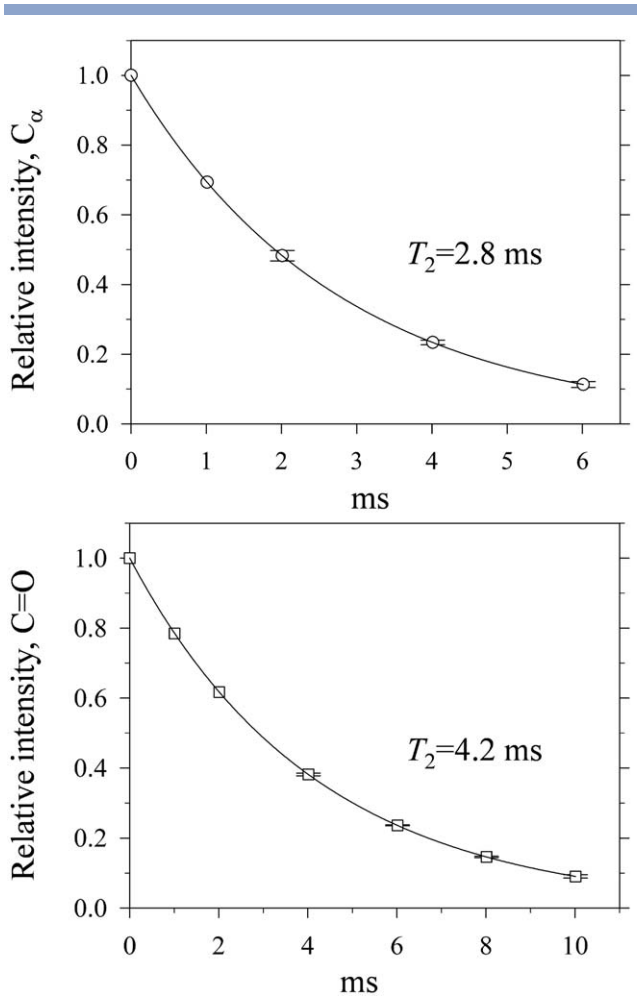

Figure 2

Spin–spin relaxation, T_2, of the ^{13}C-resonance bands of the C_α and C═O of CB_2 receptor in liposomes.

shown). Both, the ^{13}C-^{13}C- and the ^{15}N-^{13}C correlation spectra had insufficient resolution to resolve individual ^{13}C- and ^{15}N resonances. There was insufficient sensitivity to attempt 3D experiments as reported by Park *et al.* for CXCR1.[28] Several reasons may account for our lower sensitivity: (i) It appears that resolution of ^{13}C and ^{15}N resonances of CB_2 is lower which not only results in more signal superposition but also in lower sensitivity, and (ii) our lipid/protein molar ratio is higher by about a factor of 3 which resulted in a larger sample size for equal amounts of protein. The CB_2/lipid molar ratio in bilayers is limited by stringent requirements for the presence of a proper concentration of CHS in the micellar phase to protect the receptor from denaturation.[36] The CHS from the micelles ends up quantitatively in the lipid matrix which requires addition of a higher amount of phospholipids not to exceed solubility limits for CHS in proteoliposomes.[27] The use of a 3.2 mm, low-E MAS probe with a sample volume of 36 μL[28] compared to a 4-mm MAS probe with twice the sample volume in our experiments has probably resulted in higher sensitivity for the CXCR1 experiment as well. Last but not least, functional studies on reconstituted CB_2 determined that the receptor at ambient temperature and higher denatures at a rate that prevents long-lasting three-dimensional NMR experiments.[36]

Comparison to simulated spectra from a molecular model

The measured one-dimensional ^{13}C MAS NMR spectra of the agonist-bound CB_2 receptor in liposomes were compared to predicted spectra from MD simulations of CB_2 in the inactive and agonist activated states. In the course of the simulations, a spontaneous binding event of 2-AG to CB_2 was observed. The ligand entered the binding pocket located on the extracellular side of the receptor through a gap between transmembrane helices VI and VII. Ligand binding resulted in breaking of the ionic lock between arginine R3.55 and aspartic acid D6.30 located near the ends of transmembrane helices III and VI on the intracellular side of the receptor. This was followed by a side-chain flip at W6.48 that may correspond to the so-called rotamer toggle switch. Hence, the MD simulations report on atomic coordinates of the protein structure related to the critical steps of receptor activation from ligand-free inactive to agonist-bound active states. Atomic coordinates of the receptor were extracted from before 2-AG binding, after binding and breakage of the ionic lock, as well as before and after activation of the toggle switch. Each period in the evolution of the CB_2 structure was probed using five to six coordinate sets taken at 1- or 0.9-ns intervals to account

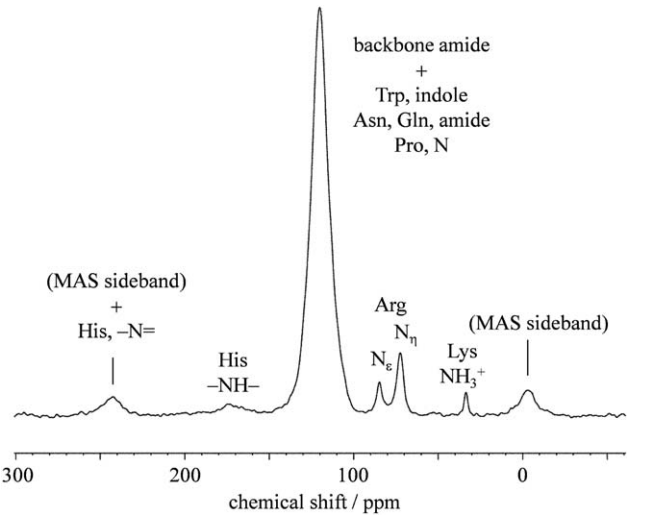

Figure 3

^{15}N MAS NMR spectrum of uniformly ^{13}C- and ^{15}N-labeled CB_2 in liposomes recorded with ^{1}H-^{15}N crosspolarization at a MAS frequency of 10 kHz.

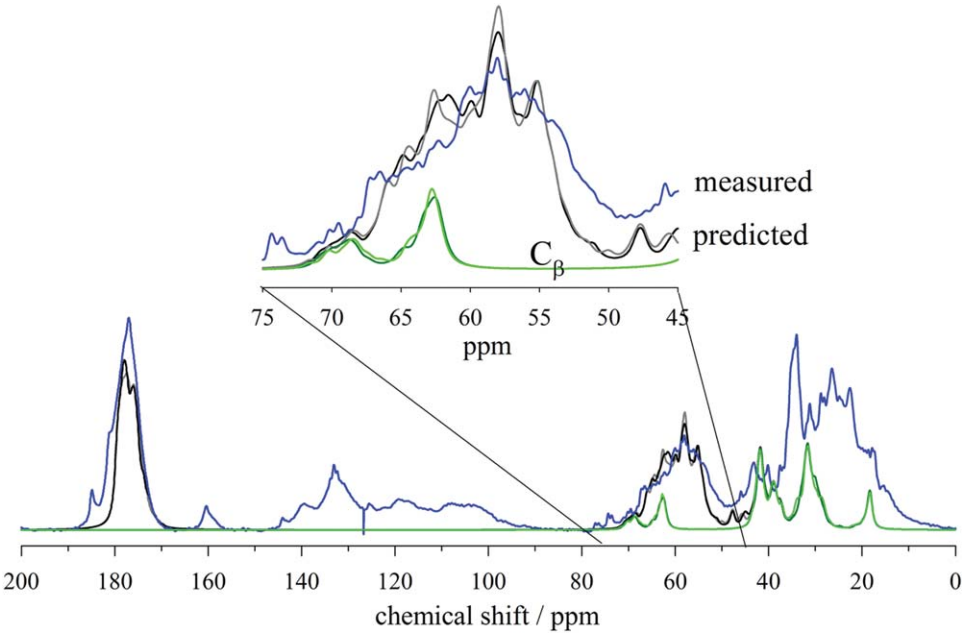

Figure 4

Comparison of the measured ^{13}C MAS NMR spectrum of the CB_2 receptor (blue) with a predicted spectrum from the MD simulations (black). The receptor is in the agonist-bound active state. The prediction was made for the backbone C_α, C═O, and side-chain C_β carbons by application of the chemical-shift prediction program SHIFTX. The predicted C_β signals were shown explicitly to specify signals from Ser (63 ppm) and Thr (69 ppm) that appear in the C_α region due to a directly bonded hydroxyl group (green). The predicted spectrum of the ligand-free inactive state of the receptor is also presented (grey) as well as the C_β signals (light green).

for rapid structural fluctuations. This allowed us to predict NMR spectral changes related to the full activation process, but also for ligand binding and breakage of the ionic lock, and for activation of the toggle switch selectively.

Chemical shifts of the backbone $^{13}C_\alpha$-, ^{13}C═O-, ^{15}NH-, and the side-chain $^{13}C_\beta$ resonances were determined from the PDB files using the programs SHIFTX and SPARTA and averaged for each time period. Differences in spectral predictions between SHIFTX and SPARTA were insignificant (Supporting Information Fig. S3). The comparison of measured and predicted spectra is shown in Figure 4. The predicted distribution of ^{13}C resonances of the fully activated state of CB_2 (black spectrum) is to be compared with the experimentally recorded ^{13}C MAS NMR spectrum in blue. It was assumed that the simulated structure of CB_2 receptor activated by 2-AG is similar to the structure of CB_2 activated by CP-55,940 in the experiment. The predicted spectrum of ligand-free, inactive CB_2 is shown as well (grey spectrum). The green spectrum shows the predicted distribution of the C_β resonances (SHIFTX and SPARTA predict only C_α, C═O, and the side-chain C_α resonances). The predicted distribution of the C_α resonances from the simulation is in decent qualitative agreement with the experimental spectrum: the experimentally measured C_α band has its highest intensity at 58.1 ppm in agreement with the predicted value of 58.0 ppm. The downfield edge of the C_α band contains also the C_β resonances of serines at 63 ppm, and threonines at 69 ppm. Their resonances are shifted downfield due to the directly bonded hydroxyl group. Inclusion of those resonances is shown to be critical for predicting the shape of the C_α band. Some differences between prediction and measurement near the upfield edge of the C_α band near 50 ppm may stem from contributions of side-chain aliphatic carbons other than the predicted C_β resonances. Thus the distribution of resonances in the C_α band can be used as an indicator of CB_2 global fold. Several more examples that indicate sensitivity of chemical shifts of the C_α region to molecular structure are shown in Supporting Information Figure S5.

Both the predicted and measured band of C═O resonances are centered at 177 ppm and have a comparable width. However, the measured C═O band includes resonances from side-chain carbonyl/carboxyl groups of asparagine (Asn), aspartic acid (Asp), glutamine (Gln), and glutamic acid (Glu) that are absent in the predicted spectrum. The standard ^{13}C chemical-shifts of side-chain carbonyl resonances (in DSS-referenced scale) measured on GGXA peptides, where X is N, D, Q, or E, are: Asn (178.3 ppm), Asp (181.2 ppm), Gln (181.7 ppm), and Glu (185.5 ppm).[56] Therefore, the visible shoulders in the measured C═O band at 181 and 185 ppm are likely

to have significant contributions from those polar side chains.

The predicted chemical shift distribution indicated small but notable differences between inactive and active states of CB_2 receptor, particularly in the distribution of intensities in the band of C_α resonances. The band intensity at 58.0 ppm decreases somewhat upon activation and an increase of intensity is predicted near 61 ppm. However, those differences would be difficult to detect in experiments using uniformly labeled CB_2 receptor, considering that the deviations between predicted and measured spectra are of similar magnitude. The predicted shape of the C═O band of resonances is almost identical for the inactive and active states except for some minor increase in intensity near 178 ppm upon activation.

To scrutinize how the intensity distribution of ^{13}C chemical shifts reflects secondary structure of the protein, we separately calculated contributions to the spectrum from (i) helices, (ii) loops, and (iii) N- and C-termini for C_α chemical shifts (Fig. 5). The helices include the transmembrane helices I-VII and the intracellular amphipathic helix VIII. The loops are rich in turns and somewhat ordered, while the N- and C-terminal domains are rich in random coil structure. It is obvious that the characteristic patterns of the experimental spectrum are determined by resonances of the helices of CB_2 that yield the characteristic maximum at 58 ppm. The upfield region of the C_α band, to the right from the maximum contains significant contributions from resonances of turns and disordered segments in the loops and the N-, and C-termini. Indeed, C_α resonances shift upfield upon a conformational transition from α-helix to random coil.[39,42,43]

It is concluded that the experimentally measured distribution of the ^{13}C-resonance intensities in the C_α region (45–70 ppm) sensitively reports the global fold of CB_2 in liposomes. The remaining deviations between the measured and predicted ^{13}C NMR spectra may have several causes: (i) The accuracy of prediction algorithms for chemical shifts of proteins has very much improved but is finite especially for comparison with chemical shifts measured by solid-state NMR.[55] (ii) The simulation of CB_2 receptor was performed on the timescale of microseconds which is unlikely to be adequate for exploration of the entire conformational space of a GPCR, although it appears that the simulations report on the most critical steps of the activation process. Furthermore, even the current simulations revealed significant motional degrees of freedom, in particular in the region of loops and the N- and C-termini. It may be necessary to conduct more extensive conformational averaging of chemical shifts using a representative set of conformations to achieve an even better agreement between experiment and simulations.[38] (iii) The CB_2 receptor in the experiment is activated by the full agonist CP-55,940 while activation in the simulation occurred by the endogenous partial agonist 2-AG. (iv) While the estimated purity of the receptor is 90% and the fraction of functionally reconstituted CB_2 receptor (>90%)[27] is rather high, the presence of some unwanted resonances may not be excluded. (v) The subtraction of natural-abundance ^{13}C-resonances of lipids from the spectra may not be perfect. With those limitations in mind, the agreement between measured and predicted ^{13}C NMR spectra of CB_2 receptor in a membrane is quite reasonable.

Changes in chemical shifts upon activation of CB_2 receptor

The availability of MD simulations of CB_2 receptor showing the effects of ligand binding, breakage of the

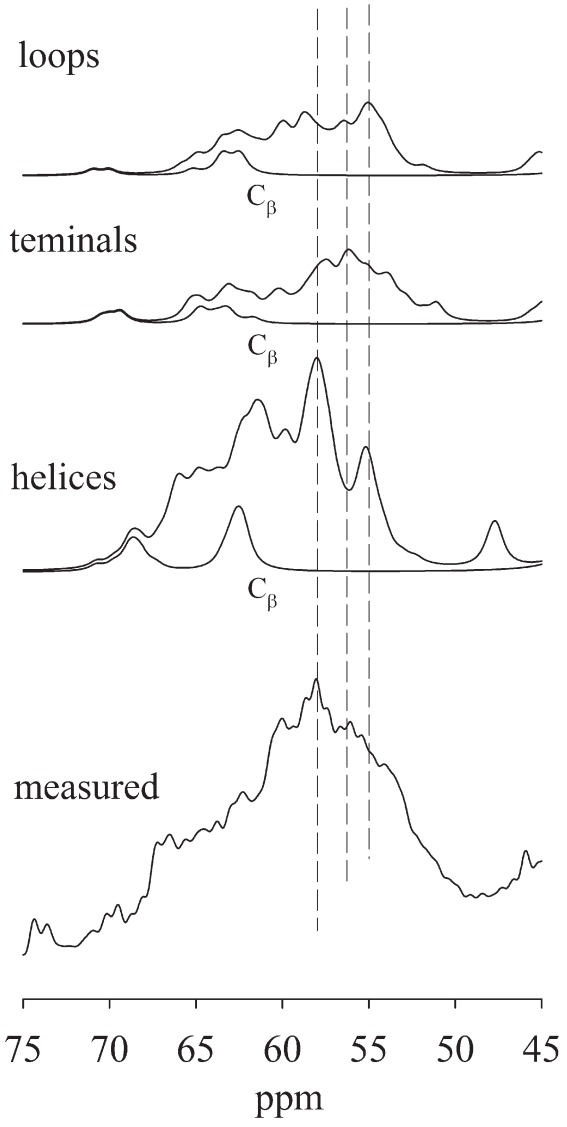

Figure 5

The C_α region of ^{13}C NMR spectra simulated for helices, N- and C-termini, and loops of CB_2 compared to the full experimentally measured spectrum. The prediction was made by the program SHIFTX using the structure of activated CB_2 obtained in MD simulations.

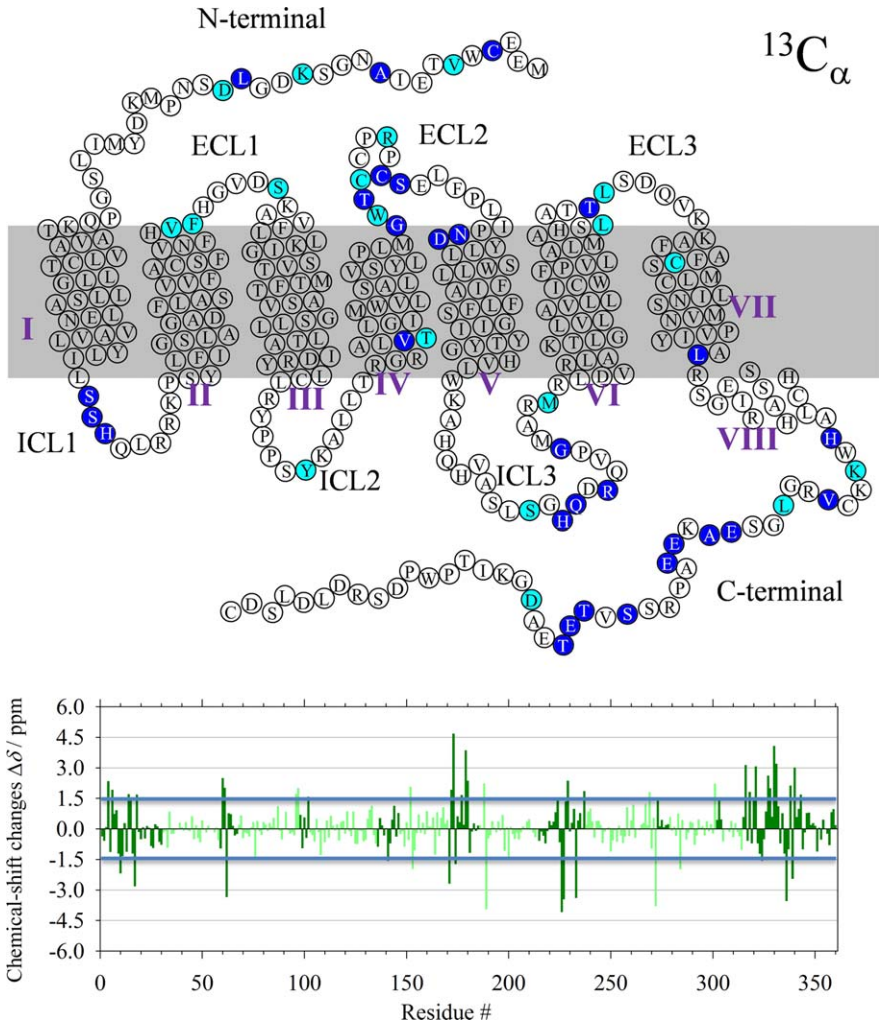

Figure 6

Predicted $^{13}C_\alpha$ chemical-shift changes ($\Delta\delta$) upon activation of CB_2 (light green, helices; green, terminals and loops). Amino acid residues with changes $\Delta\delta$ greater than ± 1.5 ppm are marked in the snake plot: 2.0 ppm $\geq |(\Delta\delta| \geq 1.5$ ppm, light blue; $|(\Delta\delta| \geq 2.0$ ppm, dark blue. The prediction was made by SHIFTX using structures generated by MD simulations. [Color figure can be viewed in the online issue, which is available at wileyonlinelibrary.com.]

ionic lock and activation of the rotamer toggle switch enabled us to predict which of the amino acid residues will experience significant changes of their ^{13}C- and ^{15}N-chemical shifts upon each of those events. Predicted changes of C_α-chemical shifts upon full activation covering several microseconds of simulation time are plotted in Figure 6 (bottom panel). The standard deviation of the chemical shift values due to fast motional fluctuations during a sampling time of about 5 ns for each of the inactive and active states was estimated to be ± 0.5 ppm on average over all C_α sites (± 0.7 ppm for the relatively flexible loops and terminals, and ± 0.4 ppm for the helices). Upon activation of the receptor significant changes of C_α-chemical shifts, larger than ± 1.5 ppm, were observed only for a limited number of C_α sites that are located primarily in the extracellular Loop 2 (ECL2), the second half of intracellular Loop 3 (ICL3), as well as in the first half of N- and C-terminal domains (top panel of Fig. 6). A similar trend was observed for C═O-, C_β-, and NH-chemical shifts (Supporting Information Figs. S6–8).

In Figures 7 and 8, the chemical shift changes for selected regions of CB_2 covering the full activation process [Figs. 7(a) and 8(a)], the binding of 2-AG and the consecutive breakage of the ionic lock [Figs. 7(b) and 8(b)], and the activation of the rotamer toggle switch [Figs. 7(c) and 8(c)] are shown. It is obvious that the critical structural events that are reflected in the chemical

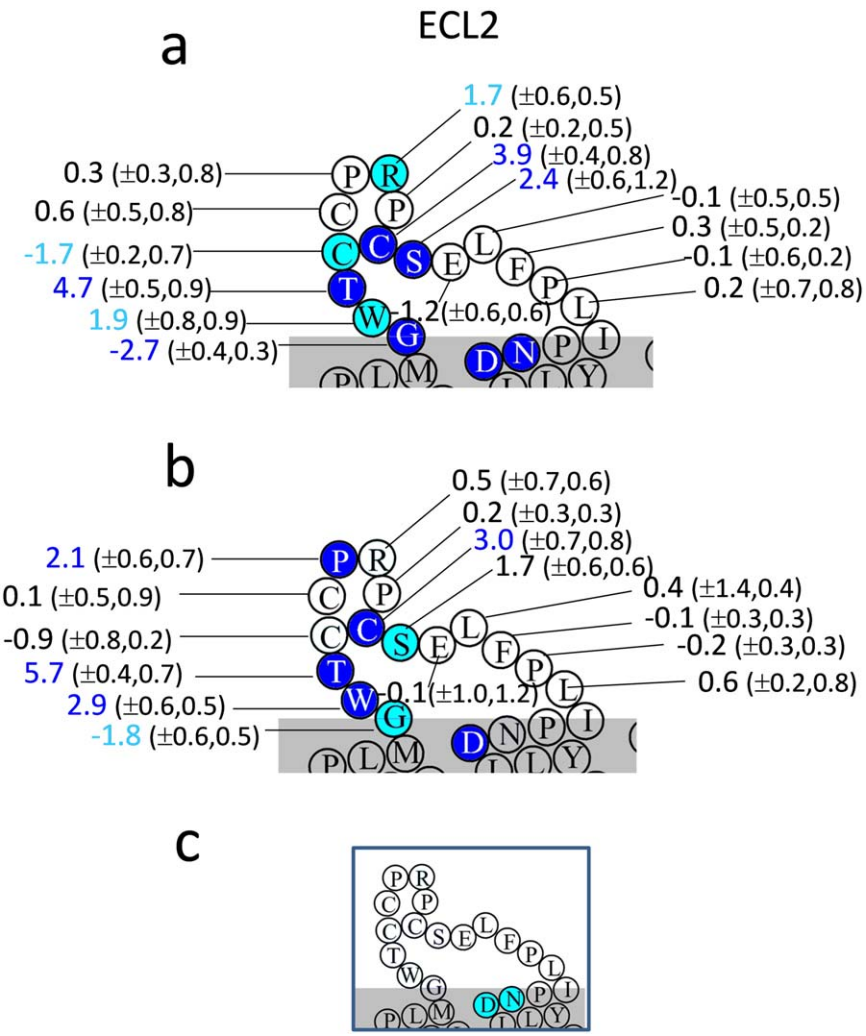

Figure 7

Predicted C_α chemical-shift changes (Δδ/ppm) of amino acid residues in the extracellular Loop 2 (ECL2) (**a**) upon activation of CB_2 receptor.[38] Amino acid residues with changes Δδ greater than ±1.5 ppm are marked in the snake plot: 2.0 ppm ≥ | Δδ| ≥ 1.5 ppm, light blue; | Δδ| ≥ 2.0 ppm, dark blue. The values in parentheses indicate the standard deviation of the chemical shift at each amino acid residue due to motional fluctuations during the 5-ns periods from inactive- (first value) and active (second value) states of the receptor, respectively. (**b**) Predicted changes (Δδ/ppm) due to 2-AG binding to the receptor pocket and the following breakage of the ionic lock between helices III and VI during the activation process.[38] (**c**) Predicted changes (Δδ/ppm) due to activation of the rotamer toggle switch at W6.48 that occurred after the breakage of the ionic lock.[38] Compared to Δδ from breakage of the ionic lock, Δδ from activation of the toggle switch are minor despite the relatively long time monitored (600 ns). [Color figure can be viewed in the online issue, which is available at wileyonlinelibrary.com.]

shift changes are the ligand binding event and the resulting breakage of the ionic lock, while activation of the toggle switch resulted in minor changes only. It is important to point out that Figures 7(a) and 8(a) cover states of the receptor separated by microseconds of simulation time. The similarities between Figures 7(a) and 8(a) and Figures 7(b) and 8(b) suggest that the biggest structural changes occurred quickly after the ligand binding event and that structural fluctuations of the receptor have a secondary influence on chemical shifts.

ECL2 is known to undergo structural changes upon receptor activation; in rhodopsin ECL2 acts like an opening lid on the retinal-binding site upon photoactivation,[59] and mutational studies on the dopamine D_2 receptor[60] and the M_3 muscarinic acetylcholine receptor[61] confirmed involvement of ECL2 in ligand binding which explains the predicted changes of ECL2 chemical shifts of CB_2 upon ligand binding (see Fig. 7).

ICL3 constitutes a critical site for binding and activation of heterotrimeric G proteins.[26] In the CB_2 simulation, ligand binding was accompanied by breaking of the

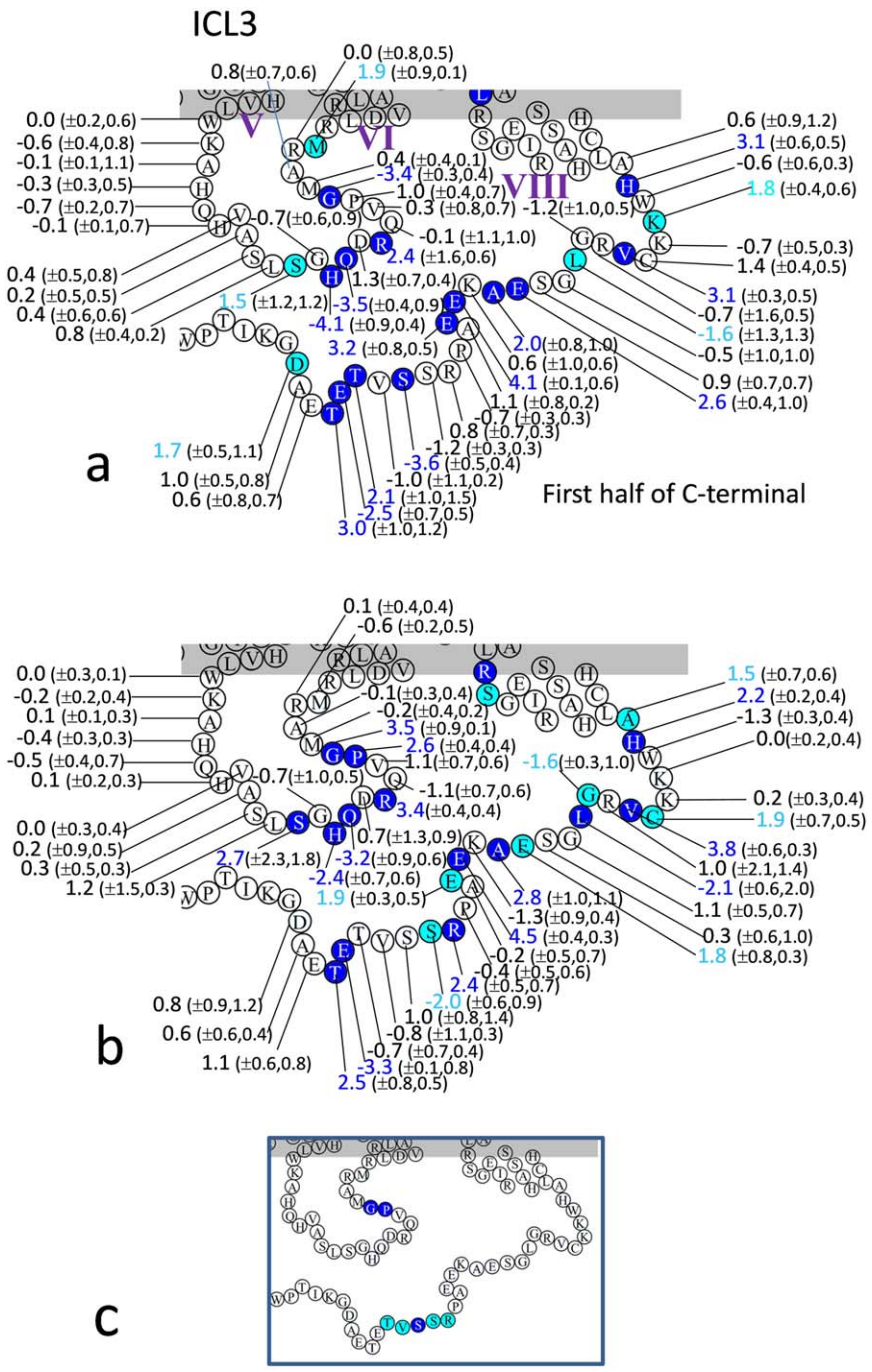

Figure 8

Predicted C_α chemical-shift changes (Δδ/ppm) of amino acid residues in the intracellular Loop 3 (ICL3) and in the first half of the C-terminal domain (**a**) upon activation of CB_2 receptor.[38] Δδ for (**b**) 2-AG binding breakage of the ionic lock, and (**c**) activation of the rotamer toggle switch as defined in Figure 7. [Color figure can be viewed in the online issue, which is available at wileyonlinelibrary.com.]

ionic lock between transmembrane helices III and VI on the cytoplasmic side of the receptor. In turn, transmembrane helix VI bends away from helix III resulting in a large movement of ICL3, which opens up the site for interaction with G protein.[38] The structural changes correlate with predicted changes of chemical shifts in ICL3 (see Fig. 8). Mutational and structural studies show that the C-terminal domain, in particular the region near helix VIII, is involved in G protein-activation as well as interactions with other signaling proteins[62]

explaining predicted changes of chemical shift in the C-terminal region. The limited number of residues undergoing notable changes of chemical shift offers themselves as suitable targets for selective amino acid labeling to study the mechanism of receptor activation by solid-state NMR.

Selection of NMR resonances according to their expected change of chemical shifts upon receptor activation must not be the sole consideration when planning selective-labeling schemes. It is also of importance to consider what kind of amino acid labeling would result in the least superposition of resonances to probe a molecular event of interest.[59,63,64] The aromatic amino acid tryptophan (Trp), for example, can be an attractive target for investigations because of its relatively low occurrence (eight) in the CB_2 receptor and its critical role in function such as toggle switch in a ligand-binding pocket.[38] Inclusion of ^{19}F-tryptophan by recombinant expression may also be utilized as a powerful NMR probe.[65] Figure 9 shows the predicted two-dimensional $^{13}C_\alpha(n)$—$^{13}C{=}O(n)$ and $^{13}C{=}O(n)$—$^{15}NH(n+1)$ correlation spectra for a specifically ^{13}C-Trp-labeled CB_2 receptor with uniform ^{15}N-labeling, corresponding to the inactive and active states [Fig. 9(a,b), respectively]. The better resolution of resonances in the $^{13}C{=}O(n)$—$^{15}NH(n+1)$ correlation spectrum is particularly useful for signal assignment. The presence of Trp-residues around the ligand binding site is also useful for locating an isotope-labeled ligand in the protein. The ^{13}C-CP-MAS NMR of ^{13}C-labeled CP-55,940 [Fig. 9(c)] in liposomes [POPC/POPS/CHS (60/15/25, mol/mol/mol)] yielded a well-resolved signal of the branched methyl groups at 28.9 ppm [Fig. 9(d)]. Considering that a method for efficient, selective Trp-labeling of CB_2 receptor has been established,[37] and that Trp is likely to be involved in ligand-binding and receptor-activation,[38] investigations on the ligand binding pocket by solid-state NMR using isotope-labeled ligands and receptor seem feasible. The NMR experiments on uniformly ^{13}C-, ^{15}N-labeled CB_2 receptor and the spectra predicted from molecular dynamics simulations on receptor activation suggest that mechanisms of receptor activation can be studied by following a limited number of resonances from selectively labeled amino acids.

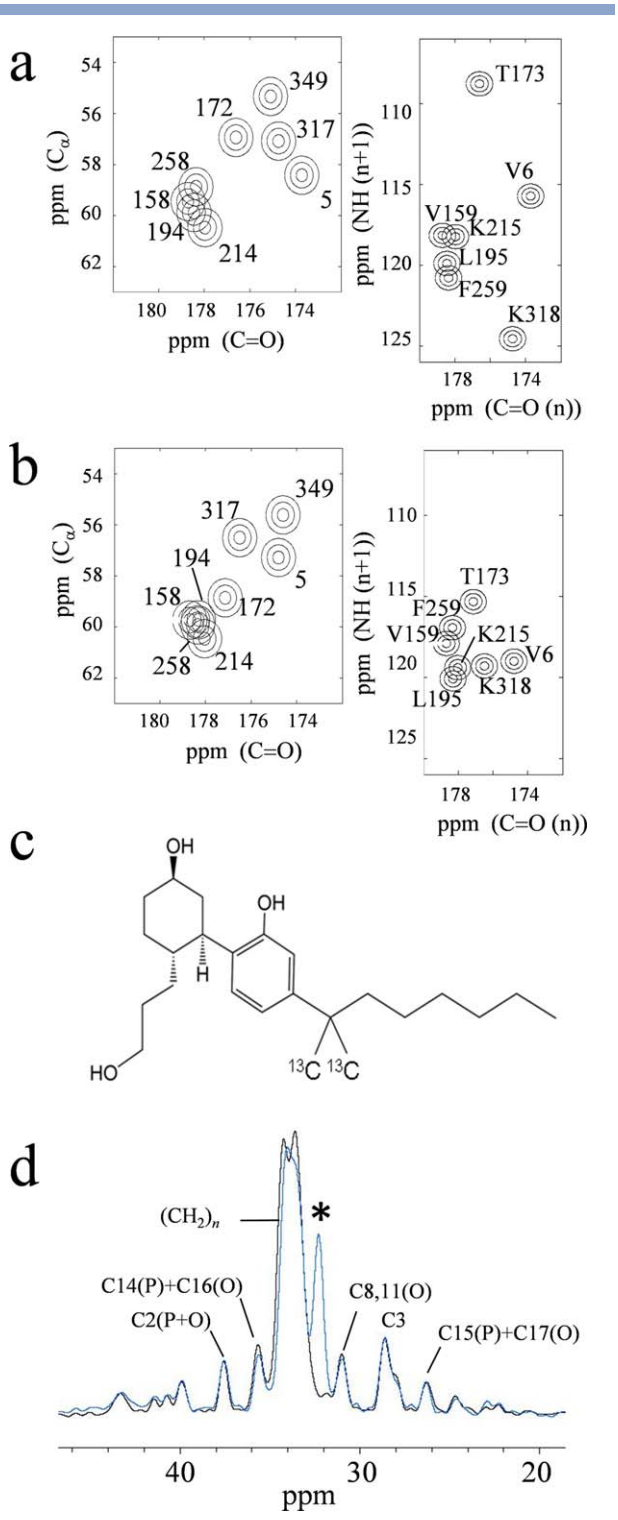

Figure 9

Two-dimensional $^{13}C_\alpha$—$^{13}C{=}O$ dipolar interaction correlation plot for Trp residues of CB_2 receptor predicted for the (**a**) ligand-free inactive and (**b**) agonist-bound active states, along with $^{13}C{=}O\ (n)$-$^{15}NH(n+1)$ dipolar interaction correlation plot for Trp(n) and the next amino acid residues ($n+1$). The spectra were predicted by SHIFTX using structures generated by MD simulations. The circles at each cross peak indicate spectral ranges corresponding to the diameters of 0.5, 1.0, and 1.5 ppm. (**c**) ^{13}C-labeled cannabinoid agonist CP-55,940 at the branched methyl groups in the nonyl tail. (**d**) ^{13}C-CP-MAS spectra of the ^{13}C-labeled CP-55,940 in liposomes [POPC/POPS/CHS (60/15/25, mol/mol/mol)] (blue), and of a liposome sample without ligand (black). The measurements were performed at 17° C and a MAS frequency of 15 kHz. The sample was prepared at a ligand/lipid ratio of 1/10 (w/w). The peak marked with an asterisk is the ligand signal. Assignments for major lipid resonances are shown.[66] [Color figure can be viewed in the online issue, which is available at wileyonlinelibrary.com.]

ACKNOWLEDGEMENTS

The authors thank Kejun Cheng and Kenner C. Rice for providing the ^{13}C-labeled CP-55,940.

Author Contributions: T.K., K.V., A.A.Y., and K.G. designed research; K.V. and A.A.Y. expressed and purified the protein; T.K. and K.G. performed NMR experiments and chemical shift analysis; D.L.L., D.P.H., A.G., M.C.P, and P.H.R. performed MD modeling and analysis; T.K., A.A.Y., P.H.R., and K.G. wrote the paper.

REFERENCES

1. Cabral GA, Griffin-Thomas L. Emerging role of the cannabinoid receptor CB2 in immune regulation: therapeutic prospects for neuroinflammation. Expert Rev Mol Med 2009;11:e3.
2. Xi Z-X, Peng X-Q, Li X, Song R, Zhang H-Y, Liu Q-R, Yang H-J, Bi G-H, Li J, Gardner EL. Brain cannabinoid CB2 receptors modulate cocaine's actions in mice. Nat Neurosci 2011;14:1160–1166.
3. Park JH, Scheerer P, Hofmann KP, Choe HW, Ernst OP. Crystal structure of the ligand-free G-protein-coupled receptor opsin. Nature 2008;454:183–187.
4. Palczewski K, Kumasaka T, Hori T, Behnke CA, Motoshima H, Fox BA, Le Trong I, Teller DC, Okada T, Stenkamp RE, Yamamoto M, Miyano M. Crystal structure of rhodopsin: A G protein-coupled receptor. Science 2000;289:739–745.
5. Choe H-W, Kim YJ, Park JH, Morizumi T, Pai EF, Krauss N, Hofmann KP, Scheerer P, Ernst OP. Crystal structure of metarhodopsin II. Nature 2011;471:651–655.
6. Jaakola VP, Griffith MT, Hanson MA, Cherezov V, Chien EYT, Lane JR, Ijzerman AP, Stevens RC. The 2.6 Angstrom Crystal Structure of a Human A(2A) Adenosine Receptor Bound to an Antagonist. Science 2008;322:1211–1217.
7. Cherezov V, Rosenbaum DM, Hanson MA, Rasmussen SGF, Thian FS, Kobilka TS, Choi HJ, Kuhn P, Weis WI, Kobilka BK, Stevens RC. High-resolution crystal structure of an engineered human beta(2)-adrenergic G protein-coupled receptor. Science 2007;318:1258–1265.
8. Warne T, Serrano-Vega MJ, Baker JG, Moukhametzianov R, Edwards PC, Henderson R, Leslie AGW, Tate CG, Schertler GFX. Structure of a beta(1)-adrenergic G-protein-coupled receptor. Nature 2008;454:486-U482.
9. Wu BL, Chien EYT, Mol CD, Fenalti G, Liu W, Katritch V, Abagyan R, Brooun A, Wells P, Bi FC, Hamel DJ, Kuhn P, Handel TM, Cherezov V, Stevens RC. Structures of the CXCR4 chemokine GPCR with small-molecule and cyclic peptide antagonists. Science 2010;330:1091–1095.
10. Chien EYT, Liu W, Zhao QA, Katritch V, Han GW, Hanson MA, Shi L, Newman AH, Javitch JA, Cherezov V, Stevens RC. Structure of the human dopamine D3 receptor in complex with a D2/D3 selective antagonist. Science 2010;330:1091–1095.
11. Haga K, Kruse AC, Asada H, Yurugi-Kobayashi T, Shiroishi M, Zhang C, Weis WI, Okada T, Kobilka BK, Haga T, Kobayashi T. Structure of the human M2 muscarinic acetylcholine receptor bound to an antagonist. Nature 2012;482:547–551.
12. Kruse AC, Hu JX, Pan AC, Arlow DH, Rosenbaum DM, Rosemond E, Green HF, Liu T, Chae PS, Dror RO, Shaw DE, Weis WI, Wess J, Kobilka BK. Structure and dynamics of the M3 muscarinic acetylcholine receptor. Nature 2012;482:552–556.
13. Hanson MA, Roth CB, Jo EJ, Griffith MT, Scott FL, Reinhart G, Desale H, Clemons B, Cahalan SM, Schuerer SC, Sanna MG, Han GW, Kuhn P, Rosen H, Stevens RC. Crystal Structure of a Lipid G Protein-Coupled Receptor. Science 2012;335:851–855.
14. Shimamura T, Shiroishi M, Weyand S, Tsujimoto H, Winter G, Katritch V, Abagyan R, Cherezov V, Liu W, Han GW, Kobayashi T, Stevens RC, Iwata S. Structure of the human histamine H-1 receptor complex with doxepin. Nature 2011;475:65–70.
15. Thompson AA, Liu W, Chun E, Katritch V, Wu HX, Vardy E, Huang XP, Trapella C, Guerrini R, Calo G, Roth BL, Cherezov V, Stevens RC. Structure of the nociceptin/orphanin FQ receptor in complex with a peptide mimetic. Nature 2012;485:395–399.
16. Manglik A, Kruse AC, Kobilka TS, Thian FS, Mathiesen JM, Sunahara RK, Pardo L, Weis WI, Kobilka BK, S. G. Crystal structure of the mu-opioid receptor bound to a morphinan antagonist. Nature 2012;485:321–326.
17. Wu H, Wacker D, Mileni M, Katritch V, Han GW, Vardy E, Liu W, Thompson AA, Huang X-P, Carrol FI, Mascarella SW, Westkaemper RB, Mosier PD, Roth BL, Cherezov V, Stevens RC. Structure of the human kappa-opioid receptor in complex with JDTic. Nature 2012;485:327–332.
18. Granier S, Manglik A, Kruse AC, Kobilka TS, Thian FS, Weis WI, Kobilka BK. Structure of the delta-opioid receptor bound to naltrindole. Nature 2012;485:400–404.
19. Zhang C, Srinivasan Y, Arlow DH, Fung JJ, Palmer D, Zheng YW, Green HF, Pandey A, Dror RO, Shaw DE, Weis WI, Coughlin SR, Kobilka BK. High-resolution crystal structure of human protease-activated receptor 1. Nature 2012;492:387–392.
20. White JF, Noinaj N, Shibata Y, Love J, Kloss B, Xu F, Gvozdenovic-Jeremic J, Shah P, Shiloach J, Tate CG, Grisshammer R. Structure of the agonist-bound neurotensin receptor. Nature 2012;490:508–513.
21. Wang C, Jiang Y, Ma J, Wu H, Wacker D, Katritch V, Han GW, Liu W, Huang XP, Vardy E, McCorvy JD, Gao X, Zhou XE, Melcher K, Zhang C, Bai F, Yang H, Yang L, Jiang H, Roth BL, Cherezov V, Stevens RC, Xu HE. Structural basis for molecular recognition at serotonin receptors. Science 2013;340:610–614.
22. Wacker D, Wang C, Katritch V, Han GW, Huang XP, Vardy E, McCorvy JD, Jiang Y, Chu M, Siu FY, Liu W, Xu HE, Cherezov V, Roth BL, Stevens RC. Structural features for functional selectivity at serotonin receptors. Science 2013;340:615–619.
23. Wang C, Wu H-X, Katritch V, Han GW, Huang X-P, Liu W, Siu FY, Roth BL, Cherezov V, Stevens RC. Structure of the human smoothened receptor bound to an antitumour agent. Nature 2013;497:338–343.
24. Siu FY, He M, de Graaf C, Han GW, Yang D, Zhang Z, Zhou C, Xu Q, Wacker D, Joseph JS, Liu W, Lau J, Cherezov V, Katritch V, Wang M-W, Stevens RC. Structure of the human glucagon class B G-protein-coupled receptor. Nature 2013;499:444–449.
25. Chung KY, Rasmussen SGF, Liu T, Li S, DeVree BT, Chae PS, Calinski D, Kobilka BK, Woods VL, Sunahara RK. Conformational changes in the G protein Gs induced by the beta(2) adrenergic receptor. Nature 2011;477:611–615.
26. Rasmussen SGF, DeVree BT, Zou Y, Kruse AC, Chung KY, Kobilka TS, Thian FS, Chae PS, Pardon E, Calinski D, Mathiesen JM, Shah STA, Lyons JA, Caffrey M, Gellman SH, Steyaert J, Skiniotis G, Weis WI, Sunahara RK, Kobilka BK. Crystal structure of the beta(2) adrenergic receptor-G_s protein complex. Nature 2011;477:549–557.
27. Kimura T, Yeliseev AA, Vukoti K, Rhodes SD, Cheng K, Rice KC, Gawrisch K. Recombinant cannabinoid type 2 receptor in liposome model activates G protein in response to anionic lipid constituents. J Biol Chem 2012;287:4076–4087.
28. Park SH, Das BB, Casagrande F, Tian Y, Nothnagel HJ, Chu MN, Kiefer H, Maier K, De Angelis AA, Marassi FM, Opella SJ. Structure of the chemokine receptor CXCR1 in phospholipid bilayers. Nature 2012;491:779–783.
29. Hassaine G, Wagner R, Kempf J, Cherouati N, Hassaine N, Prual C, Andre N, Reinhart C, Pattus F, Lundstrom K. Semliki Forest virus vectors for overexpression of 101 G protein-coupled receptors in mammalian host cells. Protein Expr Purif 2006;45:343–351.
30. McCusker EC, Bane SE, O'Malley MA, Robinson AS. Heterologous GPCR expression: A bottleneck to obtaining crystal structures. Biotechnol Prog 2007;23:540–547.

31. Chelikani P, Reeves PJ, Rajbhandary UL, Khorana HG. The synthesis and high-level expression of a beta(2)-adrenergic receptor gene in a tetracycline-inducible stable mammalian cell line. Protein Sci 2006;15:1433–1440.
32. Kimura T, Cheng K, Rice KC, Gawrisch K. Location, Structure, and Dynamics of the Synthetic Cannabinoid Ligand CP-55,940 in Lipid Bilayers. Biophys J 2009;96:4916–4924.
33. Yeliseev AA, Wong KK, Soubias O, Gawrisch K. Expression of human peripheral cannabinoid receptor for structural studies. Protein Sci 2005;14:2638–2653.
34. Krepkiy D, Gawrisch K, Yeliseev A. Expression and purification of CB2 for NMR studies in micellar solution. Protein Peptide Lett 2007;14:1031–1037.
35. Yeliseev A, Zoubak L, Gawrisch K. Use of dual affinity tags for expression and purification of functional peripheral cannabinoid receptor. Protein Expr Purif 2007;53:153–163.
36. Vukoti K, Kimura T, Macke L, Gawrisch K, Yeliseev A. Stabilization of functional recombinant cannabinoid receptor CB2 in detergent micelles and lipid bilayers. PLOS ONE 2012;7:e46290.
37. Berger C, Ho JTC, Kimura T, Hess S, Gawrisch K, Yeliseev A. Preparation of stable isotope-labeled peripheral cannabinoid receptor CB2 by bacterial fermentation. Protein Expres Purif 2010;70:236–247.
38. Hurst DP, Grossfield A, Lynch DL, Feller S, Romo TD, Gawrisch K, Pitman MC, Reggio PH. A lipid pathway for ligand binding is necessary for a cannabinoid G protein-coupled receptor. J Biol Chem 2010;285:17954–17964.
39. Ando I, Saito H, Tabeta R, Shoji A, Ozaki T. Conformation-dependent C-13 NMR chemical shifts of poly(L-alanine) in the solid state: FPT INDO calculation of N-acetyl-N′-methyl-L-alanine amide as a model compound of poly(L-alanine). Macromolecules 1984;17:457–461.
40. Saito H. Conformation-dependent ^{13}C chemical shifts: A new means of conformational characterization as obtained by high-resolution solid-state ^{13}C NMR. Magn Reson Chem 1986;24:835–852.
41. Glushka J, Lee M, Coffin S, Cowburn D. N-15 chemical shifts of backbone amides in bovine pancreatic trypsin inhibitor and apamin. J Am Chem Soc 1989;111:7716–7722.
42. Spera S, Bax A. Empirical correlation between protein backbone conformation and C-alpha and C-beta ^{13}C nuclear magnetic resonance chemical shifts. J Am Chem Soc 1991;113:5490–5492.
43. Wishart DS, Sykes BD, Richards FM. Relationship between nuclear magnetic resonance chemical shift and protein secondary structure. J Mol Biol 1991;222:311–333.
44. Dedios AC, Pearson JG, Oldfield E. Secondary and tertiary structural effects on protein NMR chemical shifts: An ab initio approach. Science 1993;260:1491–1496.
45. Le HB, Oldfield E. Correlation between N-15 NMR chemical shifts in proteins and secondary structure. J Biomol NMR 1994;4:341–348.
46. Zhang R, Hurst DP, Barnett-Norris J, Reggio PH, Song ZH. Cysteine 2.59(89) in the Second Transmembrane Domain of Human Cb2 Receptor Is Accessible within the Ligand Binding Crevice: Evidence for Possible Cb2 Deviation from a Rhodopsin Template. Mol Pharmacol 2005;68:69–83.
47. Nebane NM, Hurst DP, Carrasquer CA, Qiao Z, Reggio PH, Song ZH. Residues accessible in the binding-site crevice of transmembrane helix 6 of the CB2 cannabinoid receptor. Biochemistry 2008;47:13811–13821.
48. Tao Q, McAllister SD, Andreassi J, Nowell KW, Cabral GA, Hurst DP, Bachtel K, Ekman MC, Reggio PH, Abood ME. Role of a conserved lysine residue in the peripheral cannabinoid receptor (CB2): evidence for subtype specificity. Mol Pharmacol 1999;55:605–613.
49. Song ZH, Slowey CA, Hurst DP, Reggio PH. The difference between the CB(1) and CB(2) cannabinoid receptors at position 5.46 is crucial for the selectivity of WIN55212-2 for CB(2). Mol Pharmacol 1999;56:834–840.
50. Pei Y, Mercier RW, Anday JK, Thakur GA, Zvonok AM, Hurst D, Reggio PH, Janero DR, Makriyannis A. Ligand-binding architecture of human CB2 cannabinoid receptor: evidence for receptor subtype-specific binding motif and modeling GPCR activation. Chem Biol 2008;15:1207–1219.
51. Neal S, Nip AM, Zhang HY, Wishart DS. Rapid and accurate calculation of protein ^{1}H-, ^{13}C- and ^{15}N chemical shifts. J Biomol NMR 2003;26:215–240.
52. Shen Y, Bax A. Protein backbone chemical shifts predicted from searching a database for torsion angle and sequence homology. J Biomol NMR 2007;38:289–302.
53. Forbes J, Bowers J, Shan X, Moran L, Oldfield E, Moscarello MA. Some new developments in solid-state nuclear magnetic resonance spectroscopic studies of lipids and biological membranes, including the effects of cholesterol in model and natural systems. J Chem Soc, Faraday Trans 1 1988;84:3821–3849.
54. Morcombe CR, Zilm KW. Chemical shift referencing in MAS solid state NMR. J Magn Reson 2003;162:479–486.
55. Seidel K, Etzkorn M, Schneider R, Ader C, Baldus M. Comparative analysis of NMR chemical shift predictions for proteins in the solid phase. Solid State Nucl Magn Reson 2009;35:235–242.
56. Richarz R, Wüthrich K. ^{13}C NMR chemical shifts of the common amino acid residues measured in aqueous solutions of the linear tetrapeptides H-Gly-Gly-X-L-Ala-OH. Biopolymers 1978;17:2133–2141.
57. Takegoshi K, Nakamura S, Terao T. ^{13}C- ^{1}H dipolar-assisted rotational resonance in magic-angle spinning NMR. Chem Phys Lett 2001;344:631–637.
58. Lewandowski JR, De Paepe G, Griffin RG. Proton assisted insensitive nuclei cross polarization. J Am Chem Soc 2007;129:728–729.
59. Ahuja S, Hornak V, Yan ECY, Syrett N, Goncalves JA, Hirshfeld A, Ziliox M, Sakmar TP, Sheves M, Reeves PJ, Smith SO, Eilers M. Helix movement is coupled to displacement of the second extracellular loop in rhodopsin activation. Nat Struct Mol Biol 2009;16:168–175.
60. Shi L, Javitch JA. The second extracellular loop of the dopamine D-2 receptor lines the binding-site crevice. Proceed Nat Acad Sci USA 2004;101:440–445.
61. Scarselli M, Li B, Kim S-K, Wess J. Multiple residues in the second extracellular loop are critical for M-3 muscarinic acetylcholine receptor activation. J Biol Chem 2007;282:7385–7396.
62. Bockaert J, Marin P, Dumuis A, Fagni L. The 'magic tail' of G protein-coupled receptors: an anchorage for functional protein networks. FEBS Lett 2003;546:65–72.
63. Liu JJ, Horst R, Katritch V, Stevens RC, Wüthrich K. Biased Signaling Pathways in beta(2)-Adrenergic Receptor Characterized by F-19-NMR. Science 2012;335:1106–1110.
64. Nygaard R, Zou YZ, Dror RO, Mildorf TJ, Arlow DH, Manglik A, Pan AC, Liu CW, Fung JJ, Bokoch MP, Thian FS, Kobilka TS, Shaw DE, Mueller L, Prosser RS, Kobilka BK. The dynamic process of beta(2)-Adrenergic receptor activation. Cell 2013;152:532–542.
65. Anderluh G, Razpotnik A, Podlesek Z, Maček P, Separovic F, Norton RS. Interaction of the eukaryotic pore-forming cytolysin equinatoxin II with model membranes: F-19 NMR studies. J Mol Biol 2005;347:27–39.
66. Santaren JF, Rico M, Guilleme J, Ribera A. Thermal and C-13-NMR study of the dynamic structure of 1-palmitoyl-2-oleyl-sn-glycero-3-phosphocholine and 1-oleyl-2-palmitoyl-sn-glycero-3-phosphocholine in aqueous dispersions. Biochim Biophys Acta 1982;687:231–237.